Sensitivity of North American Monsoon Rainfall to Multisource Sea Surface Temperatures in MM5

J. LI AND X. GAO

Center for Hydrometeorological and Remote Sensing, Department of Civil and Environmental Engineering, University of California, Irvine, Irvine, California

R. A. MADDOX

Department of Atmospheric Science, The University of Arizona, Tucson, Arizona

S. SOROOSHIAN

Center for Hydrometeorological and Remote Sensing, Department of Civil and Environmental Engineering, University of California, Irvine, Irvine, California

(Manuscript received 29 June 2004, in final form 24 March 2005)

ABSTRACT

In this article, four continually processed sea surface temperature (SST) datasets, including the Reynolds SST (RYD), the global final analysis of skin temperature at oceans (FNL), and two Moderate Resolution Imaging Spectroradiometer (MODIS) *Aqua* SSTs retrieved from thermal infrared imagery (TIR) and midinfrared imagery (MIR), were compared. The results show variations from each other. In comparison with the RYD SST, the FNL data have $-0.5° \sim 0.5°$C perturbations, while the TIR and MIR SSTs possess larger deviations of $-2° \sim 1°$C, mainly due to algorithm and/or sensor differences in these SST datasets.

A regional model, the fifth-generation Pennsylvania State University–National Center for Atmospheric Research (Penn State–NCAR) Mesoscale Model (MM5), was used to investigate whether model atmospheric predictions, especially those concerning precipitation during the North American monsoon season, are sensitive to these SST variations. A comparison of rainfall, atmospheric height, temperature, and wind fields produced by model results, reanalysis data, and observations indicates that, at monthly scale, the model shows changes in the simulations for three consecutive years; in particular, rainfall amounts, timing, and even patterns vary at some specific regions. Forced by the MODIS *Aqua* midinfrared SST (MIR), which includes large regions with SST values lower than the conventional Reynolds SST, the MM5 rain field predictions show reduced errors over land and oceans compared to when the model is forced by other SST data. Specifically, rainfall estimates are improved over the offshore of southern Mexico, the Gulf of Mexico, the coastal regions of southern and eastern Mexico, and the southwestern U.S. monsoon active region, but only slightly improved over the monsoon core and the high-elevated Great Plains. Using MIR SST data, one is also capable of improving geopotential height and temperature fields in comparison with the reanalysis data.

1. Introduction

The North American monsoon (NAM) results from the seasonal transition in thermal contrasts between the North American continental and adjacent oceanic regions. A notable phenomenon associated with this transition is precipitation variation over North America during the monsoon season. After the monsoon system reaches the southwestern Mexico coast in mid-June and migrates northward to the southwestern United States in mid-July, rainfall increases over western Mexico and the southwestern United States, while it decreases over the Great Plains in the central United States and increases over the eastern U.S. coast (Higgins and Shi 2000; Higgins et al. 1997; Mo et al. 1997). This tripole variation in summertime rainfall over North America is associated not only with synoptic atmospheric pro-

Corresponding author address: Jialun Li, CHRS, Department of Civil and Environmental Engineering, University of California, Irvine, Irvine, CA 92697.
E-mail: jialunl@uci.edu

cesses, but also with SST variations in the central and/or eastern Pacific (Higgins et al. 1997; Carleton et al. 1990; Ting and Wang 1997), the Gulf of California (Stensrud et al. 1995), and the Gulf of Mexico (Markowski and North 2003), which are considered the main sources of water vapor for the NAM rainfall (Adams and Comrie 1997).

Based on long-term observational data, many studies have analyzed the relationship between SST and interannual NAM rainfall variability, and particularly the impacts of SST in various Pacific regions and the Gulf of California on NAM onset, dry and wet NAM types, and seesaw precipitation variations over the monsoon core and Great Plains (Hong and Kalnay 2000; Mo and Paegle 2000; Castro et al. 2001; Ting and Wang 1997; Higgins and Shi 2001). Observational analyses also show how SST variations affect intraseasonal NAM rainfall characteristics. Carleton et al. (1990) found that wet summers in Arizona are correlated with an enhanced longitudinal gradient of sea surface temperature between the Pacific coast of Baja California and the Gulf of California. Mitchell et al. (2002) have shown that high SST in the northern Gulf of California favors evaporation and low-level moisture, and thus is conducive to more rainfall in the southwestern United States. Mo (2000) and Woolnough and Slingo (2000) have suggested that an intraseasonal (22 day) mode in summertime precipitation over the southwestern United States is associated with tropical convection and finally is related to tropical SST variation. Cavazos et al. (2002) also showed that the intraseasonal rainfall pattern over eastern Arizona is correlated with SST variations.

A range of numerical models has been used in the NAM study. Yang et al. (2003) have investigated NAM rainfall using the Community Climate Model Version 3 (CCM3) and have found that "the under-representation of monsoon rainfall can be significantly reduced by using the yearly-varying AMIP [Atmospheric Model Intercomparison Project] SST." Kunkel (2003) ran a GCM with perturbed SSTs and concluded that the spatial and temporal variation of SST on a global scale may be one direct and proximate cause of the recently observed upward trend of extreme multiday-duration precipitation events in United States. On the other hand, using a coupled ocean–atmospheric GCM and ensemble simulations, Farrara and Yu (2003) found that the interannual and seasonal variations of NAM rainfall over the southwestern United States is largely associated with internal atmospheric processes and has little relationship to SST variations. However, Mitchell et al. (2002) have questioned these GCM results because GCMs fail to resolve the role of the Gulf of California, which is considered an important monsoon moisture source (Stensrud et al. 1995). In addition, the monthly varying SST forcing used in GCMs could miss certain daily and subdaily structures and characteristics of the ocean surface (Lau and Sui 1997; Weller and Anderson 1996). To study the role of the Gulf of California in NAM rainfall in seasonal scale, many studies (Anderson and Roads 2002; Gochis et al. 2002; Li et al. 2004; Liang et al. 2004) have employed regional-scale models. Further, Stensrud et al. (1995) found from their fifth-generation Pennsylvania State University–National Center for Atmospheric Research (Penn State–NCAR) Mesoscale Model (MM5) simulations that the SST in the Gulf of California is important for 24-h forecasts and that NAM rainfall could only be reproduced reasonably in their study cases if the SST in the Gulf of California was greater than 29.5°C. The Regional Atmospheric Modeling System (RAMS) simulation of Pastor et al. (2001) further discovered that even in 24–48-h forecasts, different SST sources [monthly climatological averages, data from the International Satellite Land Surface Climatology Project, and data derived from National Oceanic and Atmospheric Administration (NOAA) satellite images] could yield different precipitation amounts and locations. Using the National Centers for Environmental Prediction (NCEP)/Regional Spectral Model (RSM), Mo and Juang (2003) discussed the effects of SST in the Gulf of California on summertime monthly-to-seasonal precipitation in North America. Their 4-yr model tests concluded that the impact on rainfall of SSTs in the Gulf of California is greater along the western slopes of the Mexican Sierra Madre Occidental (SMO) and less over the southwestern United States.

In summary, both observational and numerical studies indicate that SST plays a significant (sometimes controversial) role in summer rainfall predictions over North America at various spatial and temporal scales. Therefore, we seek to determine the consequences of using various currently available SST datasets that are produced from different measurements and algorithms, which certainly show variations in SST representations. Will these variations from different SST datasets impact atmospheric fields, particularly rainfall distribution during the monsoon season, in regional mesoscale modeling? This comparative study examines four SST datasets, including the conventional Reynolds SST (RYD), the global final analysis of skin temperature at oceans (FNL), and the recently released Moderate Resolution Imaging Spectroradiometer (MODIS) *Aqua* mid-infrared SST (MIR) and thermal infrared SST (TIR), to investigate the impacts of different SST sources on regional climate simulations in the NAM season.

This article extends the preliminary results of Gao et

al. (2003), which show improved 2001 NAM rainfall simulation by using MODIS *Terra* SST forcing.

2. Methodology

a. Model

This study employed the Penn State–NCAR Mesoscale Model (Dudhia 1989). MM5 provides multiple options and schemes to represent a variety of physical processes. For summer rainfall simulations, the most important selection is the convective parameterization scheme (CPS). Many previous studies (e.g., Wang and Seaman 1997; Stensrud et al. 1995; Warner et al. 2003; Gochis et al. 2002; Guichard et al. 2003) have suggested that although performance may vary with rainfall types and model configurations, the Kain–Fritsch CPS (Kain and Fritsch 1990) produces reasonable rainfall patterns. This study used the Kain–Fritsch CPS with default plume radius setup, which may affect model results, especially over low-latitude regions (Mapes et al. 2004), along with simple ice-explicit microphysics (Dudhia 1989). The study also used other model physics schemes, including the Dudhia (1989) cloud radiation scheme, medium-range forecast (MRF) boundary layer scheme (Hong and Pan 1996), and Noah land surface model (Chen and Dudhia 2001). Twenty-eight vertical sigma layers were employed from the surface to the top of the model atmosphere at 70 mb, with 11 layers below 700 mb.

b. Numerical experiments

The numerical experiments configured the MM5 runs under the same model setup, except that SST forcing was replaced by different datasets. The simulation periods were July and August in 2002, 2003, and 2004 because 1) the NAM reaches full maturity in this 2-month period, and 2) the MODIS *Aqua* SST data started from 4 July 2002. Generally, the 2002 monsoon performed normally, with some localized features. The 2003 monsoon was dry east of Tucson, Arizona, and wet west of Tucson, while the 2004 monsoon was drier over Arizona, New Mexico, and California and the northwestern coast of Mexico than in a normal year. NCEP–NCAR reanalysis data (Kalnay et al. 1996) were used as the initial and boundary forcing data. The outer boundary values were updated every 12 h. The model was initiated at the beginning of each month and continued running for the whole month without reinitialization. Because MODIS *Aqua* SSTs started from 4 July 2002, the July 2002 model ran for 28 days.

Two-way nested domains were used in the simulation. Domain 1, which has a 75-km grid resolution, covers the whole United States, Mexico, southern Canada, Central America, northern South America (the region in Fig. 3), and the surrounding oceans, and domain 2, with a 25-km grid resolution, covers Mexico, western and central United States, and the surrounding oceanic regions of the eastern tropical Pacific Ocean and the Gulf of Mexico (the region in Fig. 6).

3. SST sources

MODIS *Aqua* SST data are derived from two types of infrared brightness temperature sensed from the *Aqua* platform: the midinfrared (3.8–4.1 μm) channels (MIR), and the thermal infrared (11–12 μm) channels (TIR). These data have been processed since 4 July 2002. The MODIS sensor was designed with higher sensitivity and better signal-to-noise ratio than the predecessor Advanced Very High Resolution Radiometer (AVHRR) onboard NOAA satellites. MODIS *Aqua* SST data can be provided at very high spatial (4.6 km) and temporal (daily) resolutions, but such data include a large proportion of missing data. The experiments used 36-km and weekly data, with linear interpolation to estimate missing values.

For comparison, this study included two other continually processed datasets: the Reynolds SST (RYD) and the NCEP final analysis of skin temperature over the oceans (FNL). The weekly 1° Reynolds SST is a merged product of SST surface observations, satellite estimates, and modeled simulations (Reynolds et al. 2002). Until now, the RYD SST has been widely used in either GCMs or mesoscale models; therefore, this study used RYD as a reference for comparison with other SST data. The FNL data were generated from skin temperature estimates collected over 6 h after the synoptic time (http://dss.ucar.edu/datasets/ds083.2) with 6-hourly and 1° resolution.

Figure 1 shows the daily zonal mean differences of FNL, TIR, and MIR corresponding to RYD in domain 1 for the 3 yr. Overall, in most regions and time periods the FNL, TIR, and MIR SSTs only deviated from RYD within a small range of ±0.5°C. FNL was about 0.5° higher than RYD in the low-latitude (<10°N) zone and the 50° latitude zone. TIR and MIR were largely lower than RYD, except for 2003 in the midlatitude zone (~30°N). In the tropical (5°N–5°S) and midlatitude (~40° ~ 50°N) zones, the differences between TIR/MIR SST minus RYD SST sometimes were as low as −1° to –3°C.

Figure 2 represents the daily mean absolute bias (MAB) of FNL, TIR, and MIR relevant to RYD over the domain-1 grids (75 km). The statistical measure of MAB was used in Wang and Seaman (1997) to evaluate MM5 performance. This figure shows that FNL showed

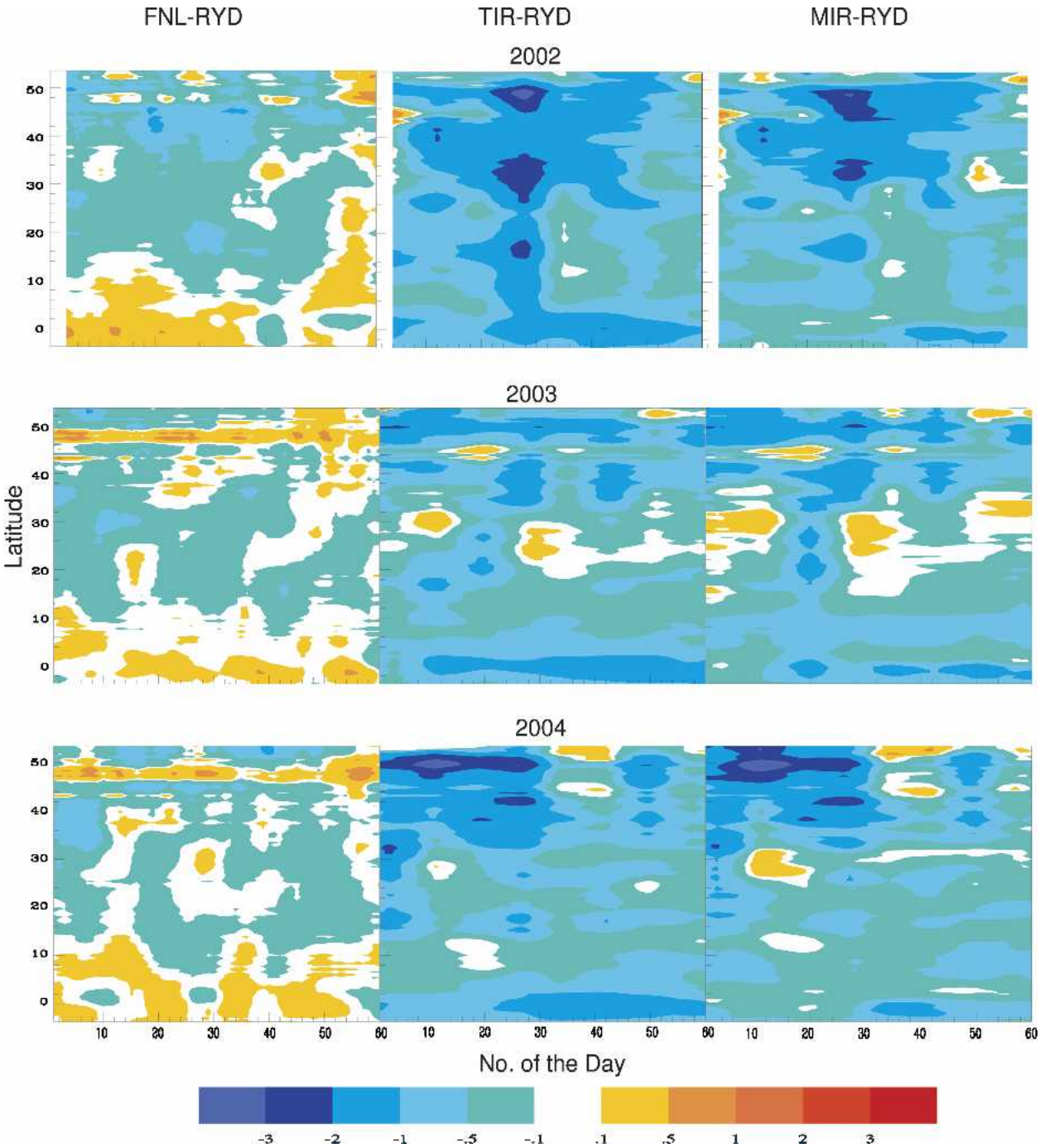

FIG. 1. Time series of zonal mean SST differences (°C) between (left) FNL and RYD, (middle) TIR and RYD, and (right) MIR and RYD during (top) Jul and Aug 2002, (middle) 2003, and (bottom) 2004.

the lowest deviation to RYD, TIR had the highest, and MIR was the median. The figure also shows that MAB amplitude decreased with time and that the daily FNL, TIR, and MIR SSTs showed 7–10-day oscillations.

Figure 3 shows maps of the differences between FNL/TIR/MIR and RYD for July and August. Again, the small-range differences in most regions indicate that while the datasets' SST magnitudes and patterns are similar, different SST sources show many variations. For the 3-yr study period, FNL was relatively high in the tropical region (0°–10°N) and low in the subtropical and extratropical regions (>10°N), except

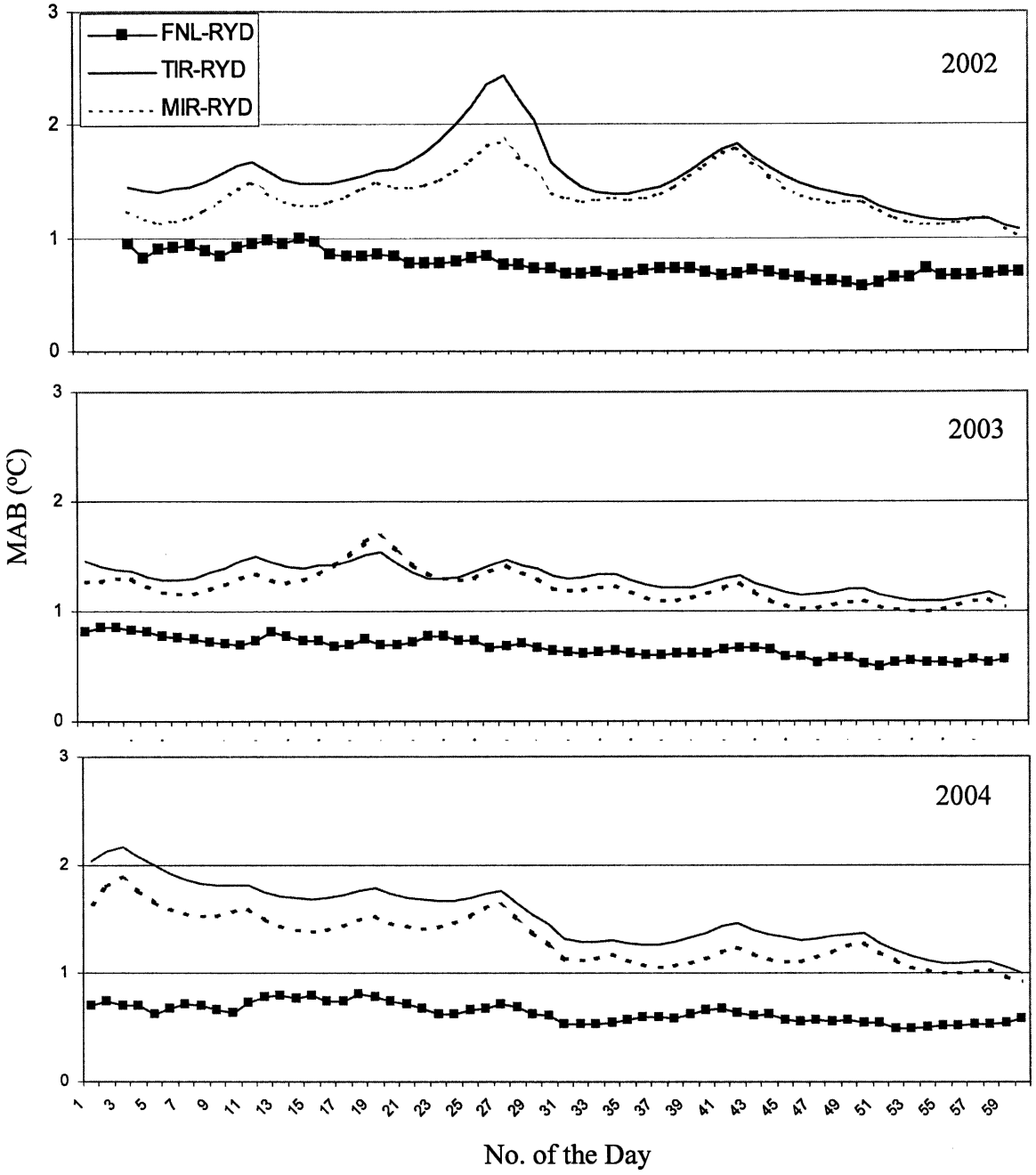

FIG. 2. Time series of daily MAB between FNL, TIR, and MIR and RYD SST datasets during the simulations.

for a high-value region in the western Atlantic Ocean offshore of the New England coast and a small low-SST zone in the equatorial eastern Pacific. Over the upper Gulf of California and offshore of the U.S. West Coast and Baja peninsula, FNL showed a narrow high-value region. In general, the differences between FNL and RYD were small, within ±0.5°C. The TIR and MIR difference maps were similar to each other but different from FNL. TIR and MIR were about 0.5° ~ 2°C lower than RYD over the most eastern Pacific, from the extratropics to the subtropics (from 55° to 5°N). However, the eastern Pacific had two high-value zones, in comparing to RYD: one located in 20° ~ 30°N and 140°W and another located in offshore of the Baja peninsula and southern Mexico. In contrast to FNL, over the tropical eastern Pacific Ocean, TIR and MIR had a "cool tong" that was 1.5°–2°C colder than RYD. In the western Atlantic Ocean, TIR and MIR were warmer

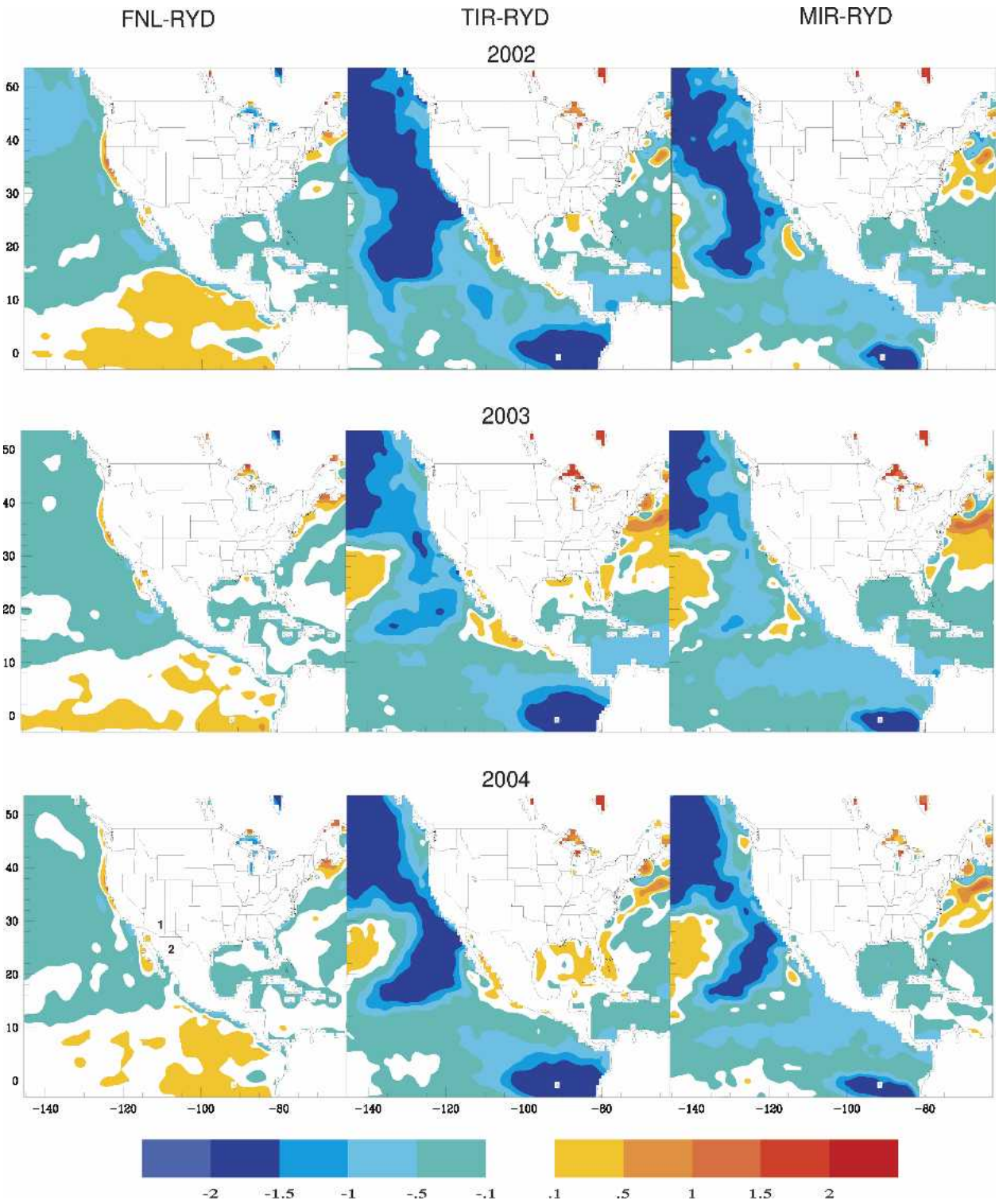

FIG. 3. SST mean difference pattern between (left) FNL and RYD, (middle) TIR and RYD, and (right) MIR and RYD during (top) Jul and Aug 2002, (middle) 2003, and (bottom) 2004. Boxes in the lower-left panel will be explained in detail later in Fig. 7 and in section 4b.

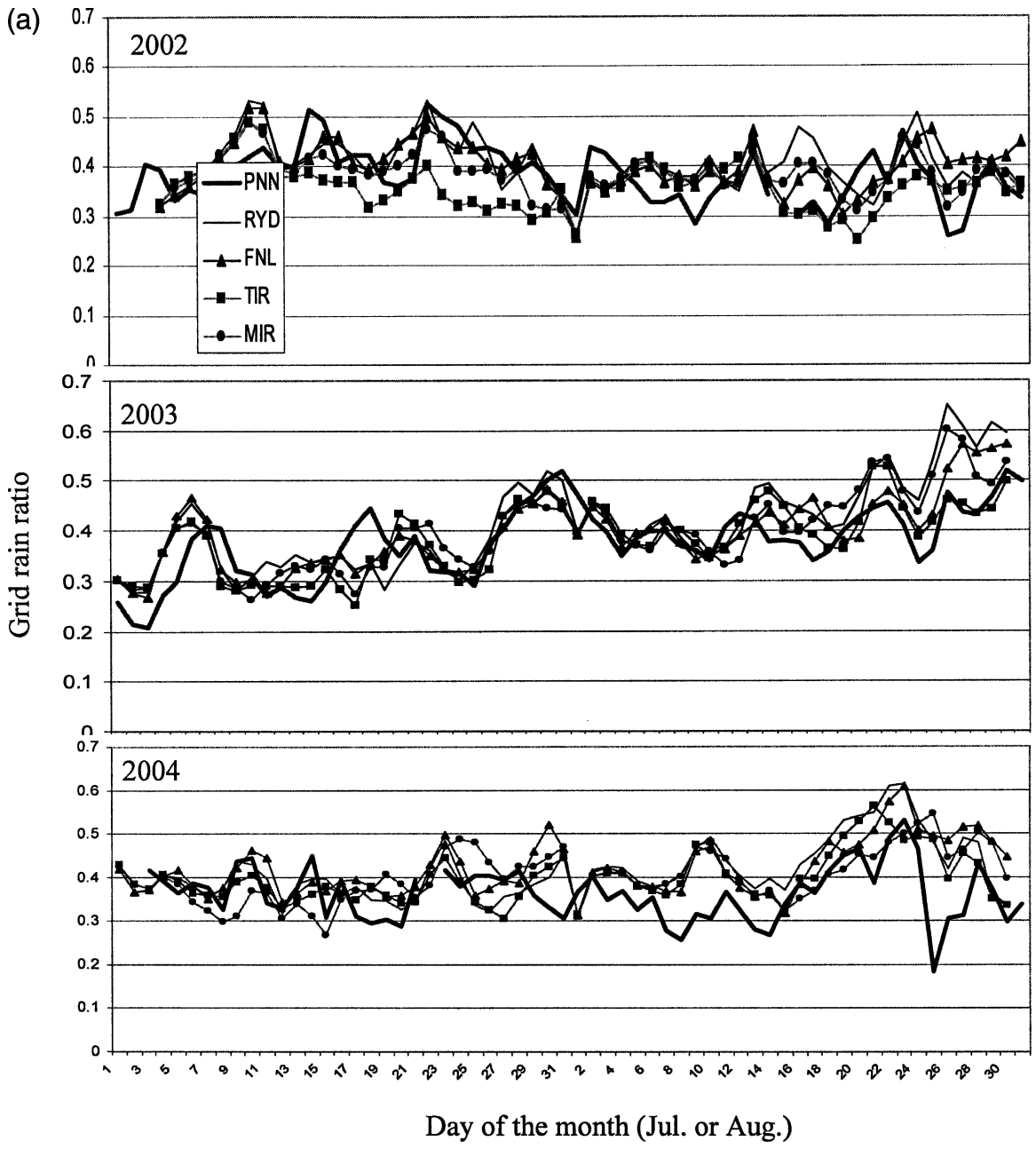

FIG. 4. (a) Mean wet day (rainfall >0.2 mm day^{-1}) time series for modeling and satellite data in domain 2.

than RYD. The differences between TIR and MIR were that in MIR, the "coolest" (dark blue) areas were less extensive than the TIR and vice versa for the "warmest" (orange) areas. In addition, MIR was the "coldest" over the Gulf of Mexico. The SST variations from different datasets were spread over certain large regions, and the patterns were consistent over the 3 yr, which suggests that the variations may result from different sensors and algorithms employed by different data sources. Currently there is lack of SST measurements to validate SST data accuracy. One question for model research concerns how such SST variations from different datasets will affect the model results. The numerical experiments were designed to investigate this question.

4. Results

a. Rainfall comparison

To examine rainfall, the model used 25 km by 25 km daily precipitation analysis data from the National

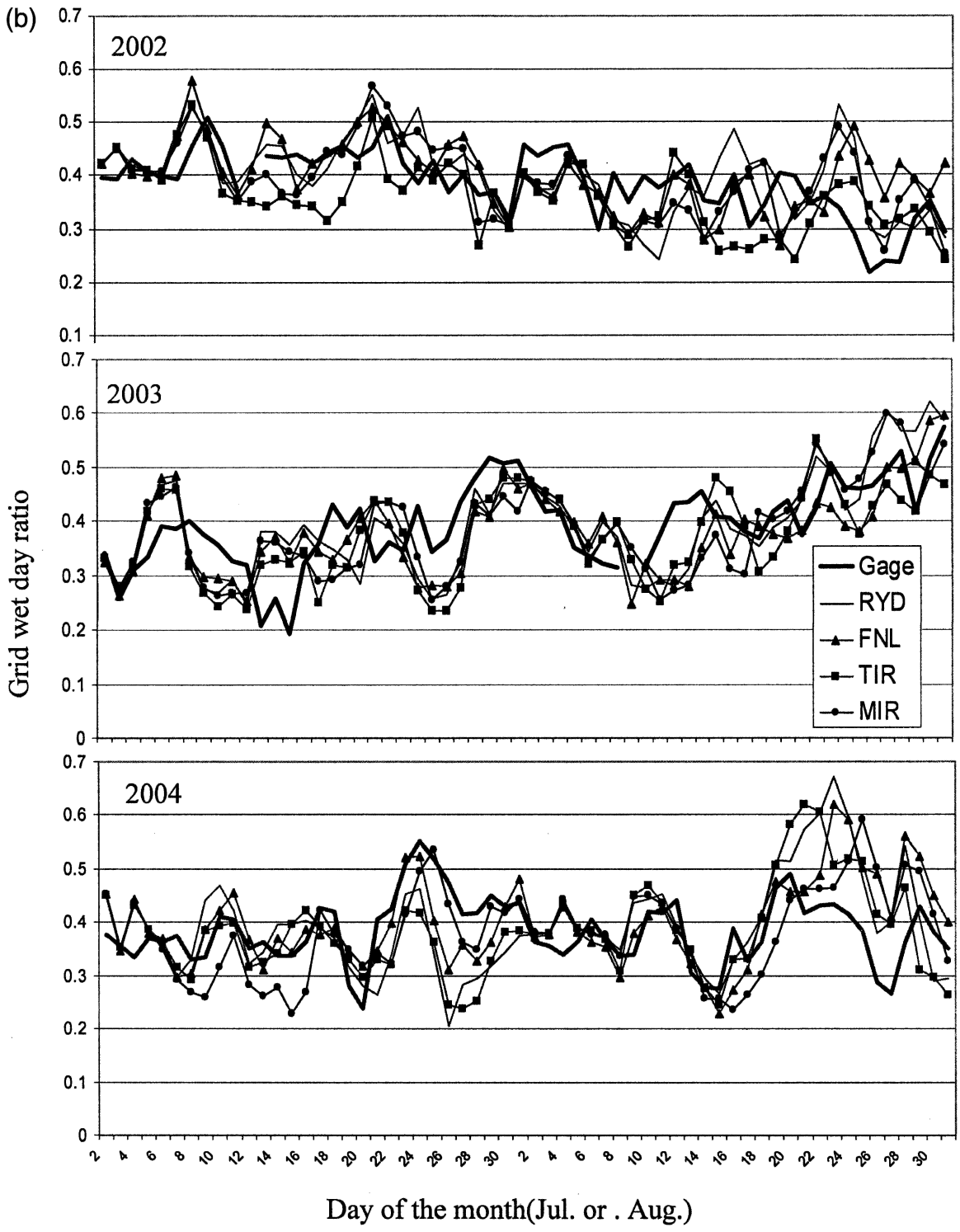

FIG. 4. (b) Mean wet-day time series for modeling and gauge data in domain 2 over land.

Weather Service/Climate Prediction Center (NWS/CPC; Higgins et al. 1999) as the observation values over land. The gauge data were interpolated from daily gauge observation and covered the United States and Mexico (for more details, see the Web site http://www.cpc.ncep.noaa.gov/products/precip/realtime). Satellite-based rainfall estimates from the Precipitation Estimation from Remotely Sensed Information using

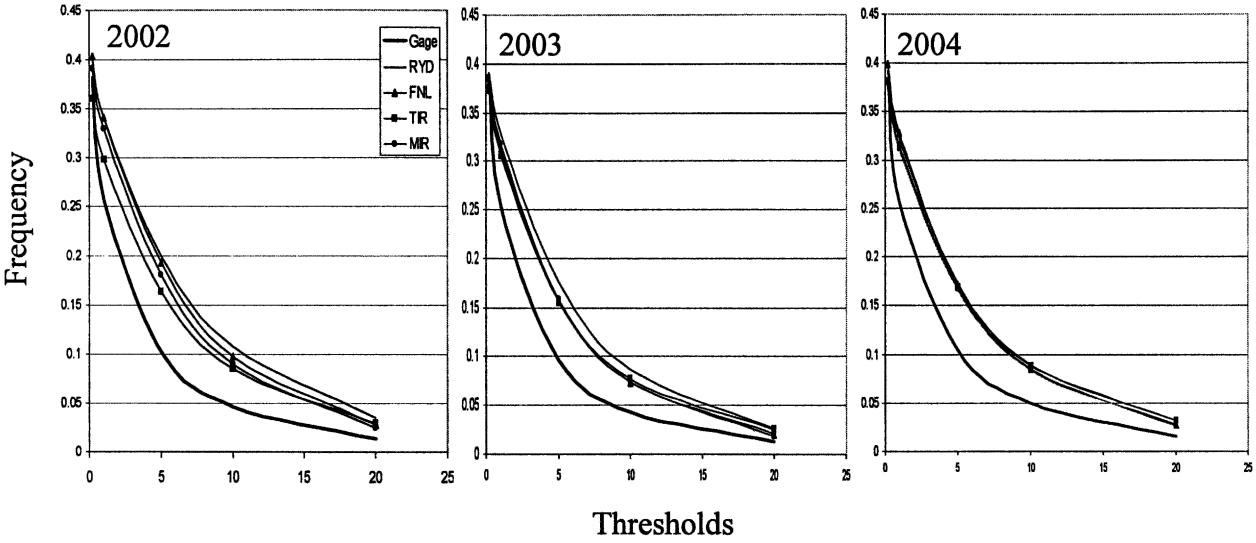

FIG. 5. Frequencies of 24-h rainfall at five thresholds (0.2, 0.5, 1.0, 5.0, 10.0, and 20.0 mm) during the 2 months for different years when different SST datasets were used.

Artificial Neural Networks (PERSIANN) system (Sorooshian et al. 2002) were employed to compare rainfall over the oceans. The PERSIANN data, retrieved from combined geostationary infrared and Tropical Rainfall Measuring Mission (TRMM) microwave information, have a global coverage at 0.25° resolutions. However, because of the mountainous topography in Mexico and the southwestern United States, the rain gauge network in the region is sparse and heterogeneous (more gauges are located in the accessible flat valleys than in the mountains), which may affect the accuracy of the rainfall data. Although satellite remotely sensed rainfall data show unprecedented, integrated global precipitation patterns, many studies (e.g., Garreaud and Wallace 1997) have noted that deficiencies in satellite rainfall estimates, namely, indirect rainfall estimates and limited rainfall sampling in space and time, can reduce the accuracy of the results. Therefore, they were used in this study as independent references, rather than as absolute foundational data, to analyze the model's performance in reproducing rainfall.

1) DAILY RAINFALL

This study used MM5 as a regional climate model for seasonal climate study; therefore, the model setup, which included 1) relatively coarse (75 km × 25 km) grid systems, and 2) model initiation only at the beginning of each month, was, in fact, inadequate to reproduce day-to-day checking rainfall, especially for mountainous regions (Li et al. 2004). This section uses statistical evaluation for the domain-2 grids (25 km). Figure 4a represents the daily time series for the ratio of rain grids (rainfall >0.2 mm day^{-1}) to total grids. In the figure, the bold line stands for the satellite-observed rain grid. The fine line, fine line with triangles, fine line with squares, and fine line with circles represent the ratio time series when RYD, FNL, TIR, and MIR, respectively, were used as SST forcing. The day was reckoned from 0000 to 0000 UTC to coordinate with the satellite daily rainfall. Except for August 2004, when the satellite rainfall estimates were perturbed for unclear reasons, the model time series generally matched the satellite variations in trend. For the first few days, the ratios were nearly the same in the four model time series, but afterward the ratios differed. Figure 4b is the same as Fig. 4a except for the comparison with the gauge rainfall observation (bold line) over land, and the day was reckoned from 1200 to 1200 UTC in order to meet the gauge daily rainfall accumulation. The figure shows the same features as in Fig. 4a. Note that in August 2004 in Fig. 4b, modeling results were comparable with the observation.

Figure 5 shows the occurrence frequencies for daily rainfall greater than five rainfall-amount thresholds (i.e., 0.2, 1.0, 5.0, 10.0, and 20.0 mm per day) in the domain-2 grids (over land only). All model rainfalls showed positive biases in comparison with the gauge data. The model rainfall forced by TIR and MIR was slightly closer to the observations than that forced by RYD and FNL.

2) MONTHLY RAINFALL

Figure 6 illustrates the differences between the modeled and observed monthly rainfall. The observed data

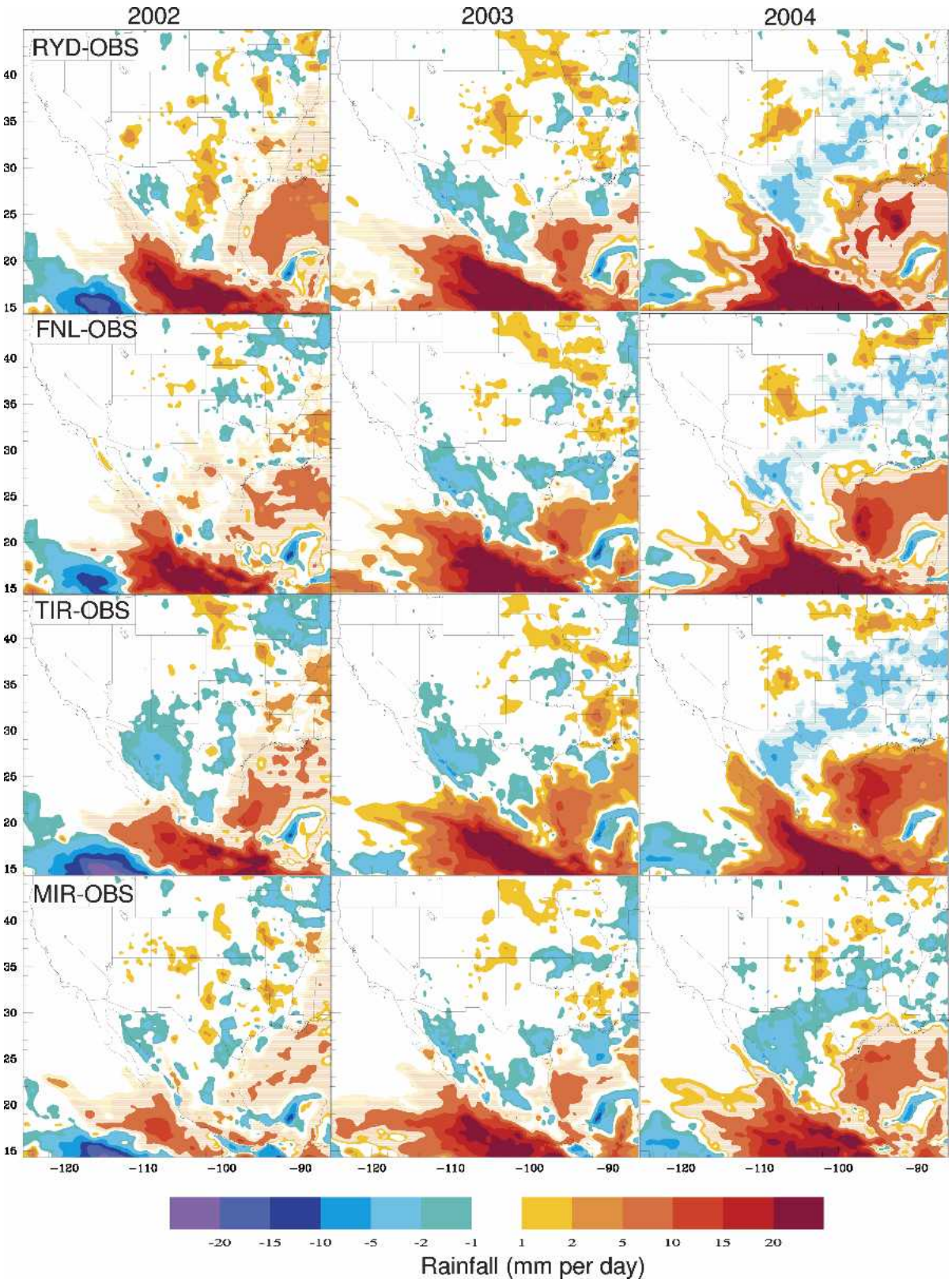

FIG. 6. Mean monthly precipitation differences between model and observation (gauge over land and PERSIANN over water) during the simulations.

TABLE 1a. Correlation between models and gauge over land in monthly scale.

		Gauge	RYD	FNL	TIR	MIR
2002	Correlation	1.0	0.62	0.63	0.57	0.70
	Mean (mm)	71	102	91	85	81
	Rms (mm)	57	118	95	116	75
2003	Correlation	1.0	0.59	0.63	0.64	0.68
	Mean (mm)	68	90	78	84	75
	Rms (mm)	58	122	99	118	83
2004	Correlation	1.0	0.5	0.52	0.46	0.56
	Mean (mm)	75	96	92	94	85
	Rms (mm)	54	127	117	130	105

consisted of the gauge rainfall over land and the PERSIANN estimates over oceans. The similarity among the rainfall difference maps in Fig. 6 results from the basic common characteristics in these SST data and the same atmospheric forcing fields. In general, the modeled rainfall (forced by any SST data) was overestimated over southern and eastern Mexico, the subtropical (15°–25°) eastern Pacific (offshore of southern Mexico), and the Gulf of Mexico, but underestimated over northwestern Mexico (the monsoon core area) and subtropical eastern Pacific. This overestimate was modest in 2002 (normal NAM year), and became more severe in 2003 and 2004 (dry NAM years). In 2004, the rainfall-underestimated area expanded from the NAM core in northwestern Mexico to the lower Great Plains. The authors checked both modeling and gauge daily rainfall and found that the model did not correctly reproduce the rainfall events that occurred at that region during late July 2004. The model performed relatively well in the southwestern United States, except for certain overestimates in the high-elevated regions (Colorado, northern New Mexico, northeastern Arizona, and southeastern Utah).

The map of Fig. 6 shows the advantages of using the MIR forcing: 1) The rainfall overestimates over the southern and eastern coasts of Mexico, the subtropical eastern Pacific, and the Gulf of Mexico were reduced substantially; 2) over the large region of northwestern Mexico (the monsoon core), northern Mexico, and central Texas to the central United States (the Great Plains), rainfall errors (overestimates/underestimates) were distributed in small areas (except for 2004); and 3) over the southwestern United States, the overestimated rainfall in the mountainous region was realistic because the gauge rainfall underestimated actual rainfall.

Table 1a (over land) and Table 1b (over oceans) list the statistics of mean, root-mean-square error (rms), and correlation coefficients between modeled and observed rainfall in the domain-2 grids. Clearly, the MIR-forced model rainfall has the closest mean, lowest rms, and highest correlation coefficient corresponding to the observations.

For checking rainfall variation in monsoon regions, Fig. 7 gives area mean diurnal variations over the southwestern U.S. monsoon active region (southeastern Arizona and southwestern New Mexico) and monsoon core (northwestern Mexico), whose locations are shown as the boxes in low left figure of Fig. 3. Box 1 in Fig. 3 is approximately 240 km by 240 km centering at (32°N, 110°W). Box 2 is the same as box 1 but centering at (27°N, 108°W). "Obs" (bold line) in the top three panels of Fig. 7 represents stage IV multisensor (gauge mixes with radar data) hourly data (http://www.joss.ucar.edu/cgi-bin//codiac/dss?21.093). For comparison with modeling results, stage IV hourly data were first added to 3 hourly, then averaged to the grid cells of

TABLE 1b. Correlation between models and PERSIANN over water in monthly scale.

		PERSIANN	RYD	FNL	TIR	MIR
2002	Correlation	1.0	0.71	0.76	0.66	0.75
	Mean (mm)	133	233	227	183	155
	Rms (mm)	188	340	329	286	192
2003	Correlation	1.0	0.76	0.74	0.77	0.73
	Mean (mm)	98	265	239	216	206
	Rms (mm)	124	401	352	347	282
2004	Correlation	1.0	0.81	0.81	0.78	0.8
	Mean (mm)	93	280	275	241	211
	Rms (mm)	127	397	397	376	288

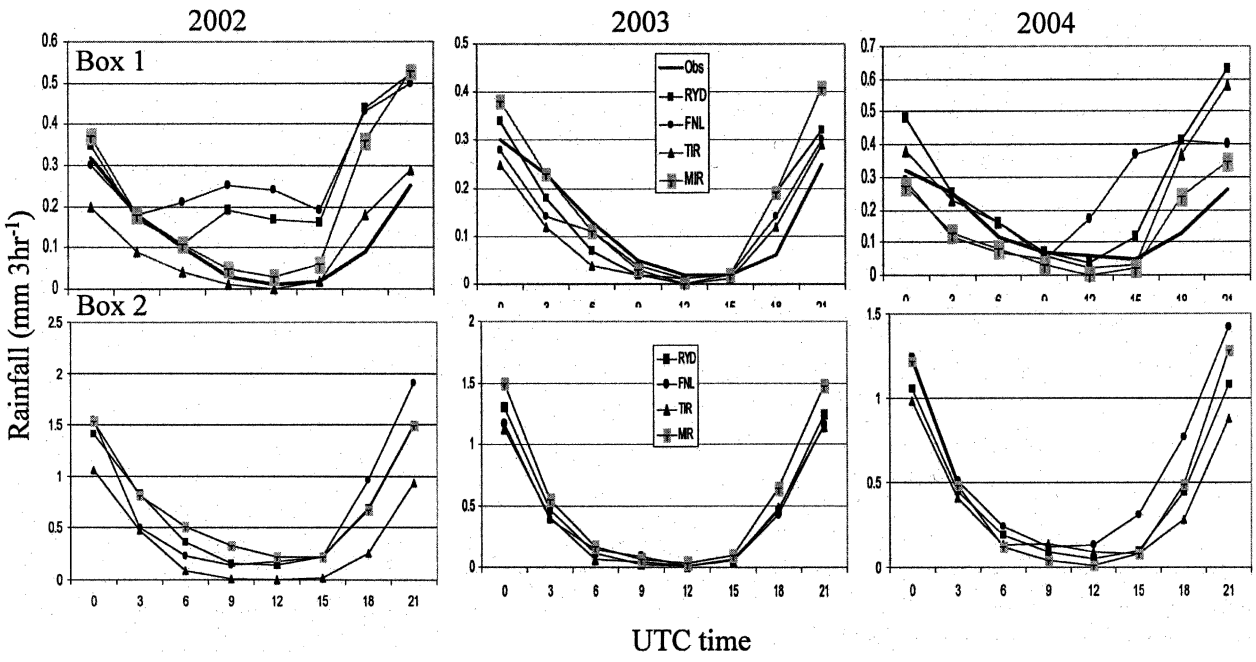

FIG. 7. Rainfall mean diurnal variations over the monsoon region. (top) Southeastern Arizona and southwestern New Mexico and (bottom) northwestern Mexico with detail in text.

domain 2 in this paper. (There is no data outside of the United States.) In 2003, all of the modeling diurnal variations have the same pattern as that of observation. However, when MODIS SST datasets were used, the modeling diurnal variation and the observation matched rather well in 2002 and 2004 while it did not when RYD and FNL datasets were used. This result again demonstrated the merit when MODIS SST datasets were used, although, at this case, the model did not exactly reproduce the intensity and beginning time and ending time of rainfall diurnal cycle. When comparing the modeling diurnal variation with stage IV data, all the modeling results cannot match the observed nighttime peaks in central United States (figures not shown) partly because the Kain–Fritsch CPS was used (Liang et al. 2004).

As shown in the bottom three panels of Fig. 7, there were nearly the same diurnal variations over the monsoon core when different SST datasets were used. This result is consistent with previous studies (i.e., Mo and Juang 2003; Stenrud et al. 1995), whose rainfall over the monsoon core is mainly affected by SST in the Gulf of California. The differences of the four types of SSTs to be employed here over the Gulf of California were relatively small (refer back to Fig. 3).

b. Surface atmospheric variables

The mean surface temperature and wind were examined monthly using NCEP–NCAR reanalysis data (NNRD) after the model results were interpolated into NNRD grids. Differences between the modeling results and NNRD for the monthly mean surface temperature over land show similar patterns, and it is unclear which particular SST dataset that was used generated a "better" result. Generally, the model overestimated most of the regions, except for Rocky Mountain areas in 2002 and 2003. The overestimated values reached 3° ~ 4°C over the southern California desert areas, the southern United States, Central American countries, and part of northern South America. Over the Rockies, the models underestimated about 0.5° ~ 1°C along northern Mexico, New Mexico, and Colorado to Montana. The 2004 results are the same as for 2002 and 2003, except that the model also underestimated the northwestern United States. Over the oceans, the model results conformed to the SST variations.

Mean wind speed differences between the models and the NNRD show the same patterns. In contrast to surface temperature differences, *U*-component wind differences occurred mainly over the oceans, especially the subtropical and tropical oceans. There was a positive bias over the eastern Pacific Ocean between 10° and 20°N. This positive bias was the largest in the simulations. Another positive bias occurred over Cuba and adjacent areas. Three negative biases were located offshore of the western U.S coast, the upper Gulf of California, and the equator cool tong regions over the eastern Pacific. The modeled-NNRD mean *V*-component

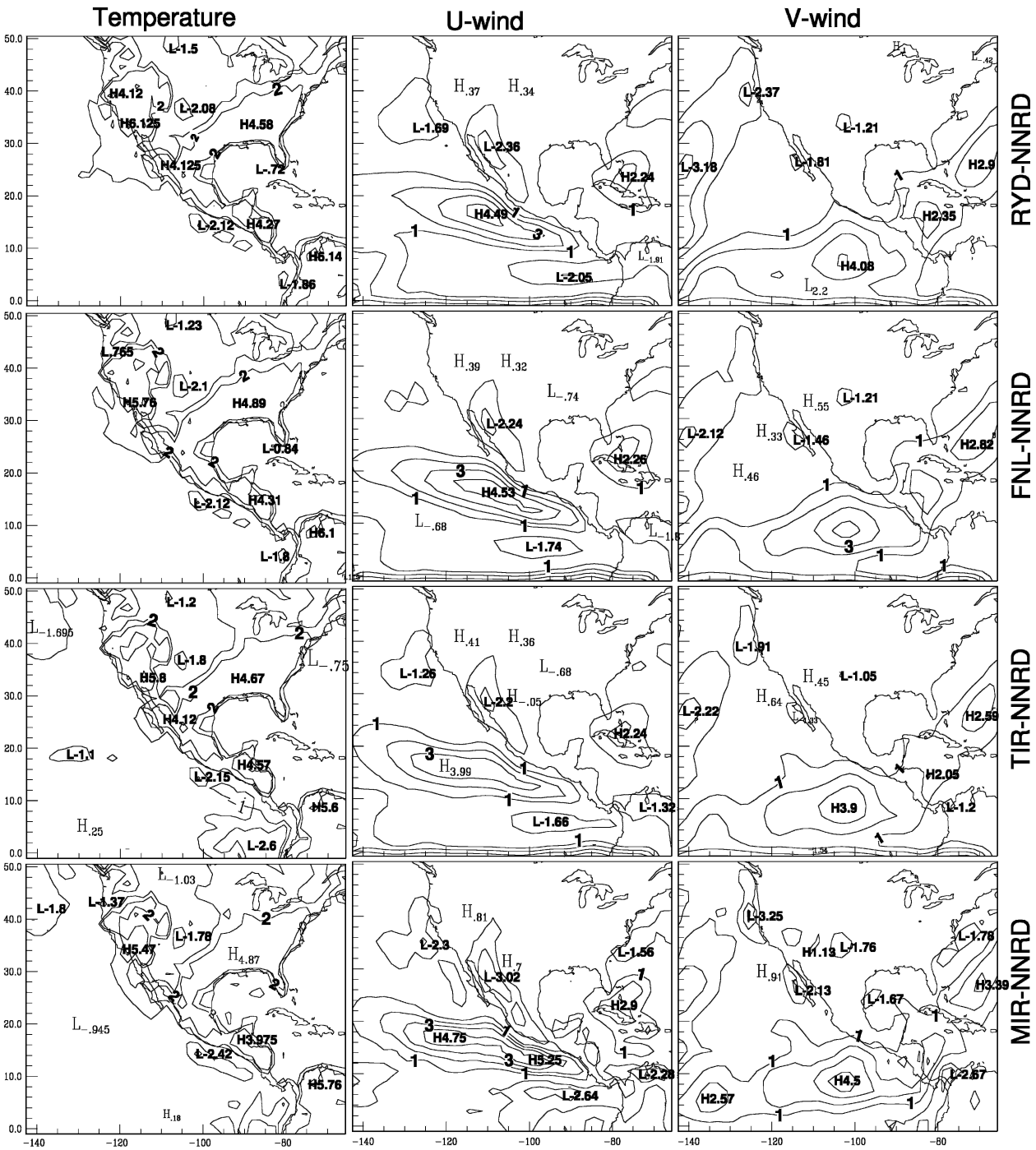

FIG. 8. Surface variable mean differences between model and NNRD in 2003. The temperature contours are −5°, −2°, −1°, 1°, 2°, and 5°C, and wind speed contours are −4, −3, −2, −1, 1, 2, 3, and 4 m s^{-1}.

differences showed the same pattern when different SST datasets were used. The positive bias pattern extends from the tropical Pacific to Cuba and finally to the western Atlantic. The greatest positive bias was located at approximately 10°N, 100°W. In addition, a negative bias extended from the middle of the western model boundary northwestward to the northwestern U.S. coastal region. Figure 8 shows the 2003 modeled-NNRD surface temperature and wind differences. The "H" and "L" labeled in the figure represent the highest and lowest differences, respectively. Finally, both surface temperature and wind near the south boundary

TABLE 2. Mean and variance of surface temperature for modeling and analysis data.

		Obs	RYD	FNL	TIR	MIR
2002	Mean (°C)	23.07	23.85	23.78	23.32	23.50
	Rms (°C)	4.44	4.26	4.31	4.54	4.48
2003	Mean (°C)	23.26	24.16	24.11	23.83	23.89
	Rms (°C)	4.28	4.26	4.30	4.43	4.36
2004	Mean (°C)	23.52	23.54	23.52	23.52	23.28
	Rms (°C)	4.72	4.38	4.39	4.39	4.51

TABLE 3b. Mean and variance of surface *V* component for modeling and analysis data.

		Obs	RYD	FNL	TIR	MIR
2002	Mean (m s^{-1})	0.04	0.58	0.56	0.44	0.47
	Rms (m s^{-1})	1.80	3.45	3.42	3.15	3.17
2003	Mean (m s^{-1})	0.12	0.77	0.73	0.64	0.65
	Rms (m s^{-1})	1.84	3.40	3.39	3.16	3.14
2004	Mean (m s^{-1})	0.24	0.83	0.82	0.74	0.72
	Rms (m s^{-1})	1.92	3.52	3.51	3.31	3.24

have a relatively strong positive bias between the models and NNRD, except when the MIR dataset was used.

Table 2 shows the modeled and NNRD surface temperature mean and rms during simulations. Table 3a and Table 3b are the same as Table 2, except for the *U* and *V* components, respectively. In summary, it is difficult to determine which SST dataset that was used to drive the model was able to generate more accurate surface meteorological fields.

c. *Atmospheric processes*

Mean modeling circulation patterns were similar but not exactly the same (figures not shown) during the simulated period when different SST types were used. At 500 mb, the subtropical high system dominated over the continent, and separate troughs were located near the eastern and western U.S. coasts. The easterly dominated in the tropical zone, while the westerly controlled in the extratropical zone.

This part of the study just summarily compared the model results with the NNRD to determine which result was relatively more accurate when different SST datasets were used at current model conditions. For detail, we will address these results separately.

Figure 9 shows the difference in mean geopotential height between the simulations and NNRD at 500 mb. The "H" and "L" represent the highest and lowest differences between the simulation and reanalysis data. When different datasets were forced, the difference patterns were very close in the same year but changed in different years. In comparison with the NNRD, the model underestimated geopotential height over the open ocean located in the southwestern lower Gulf of California during the modeling time periods. The model also underestimated the height field over the northeastern United States and/or near ocean (see the –20 m contour line in Fig. 9). In 2002 and 2003, in comparison with the NNRD, the model overestimated the height field near the western U.S. coastal region, while in 2004 the model underestimated an area over the northwestern United States. However, when the MODIS SST dataset was used, the model generated a relatively small area coverage circling the −20 m contour line and light intensity values over that area, compared to the RYD dataset.

Figure 10 shows the mean temperature differences between models and NNRD at 500 mb. Generally, the differences show very similar patterns when different SST datasets forced the model. However, comparing the 1° and 2°C contour line area-coverage with their central values shows that when the MODIS MIR SST dataset was used to drive the model, the modeling results were closer to the NNRD dataset than those when the other SST datasets were used.

In comparison with the temperature differences between modeling and NNRD in Figs. 8 and 10, it is easy to note that in the lower level, the gradient of the difference is bigger than that in the higher level, partly because the NNRD dataset cannot represent the strong local characteristics caused by land features like land use and topography.

TABLE 3a. Mean and variance of surface *U* component for modeling and analysis data.

		Obs	RYD	FNL	TIR	MIR
2002	Mean (m s^{-1})	−1.03	−0.45	−0.58	−0.46	−0.61
	Rms (m s^{-1})	2.68	2.23	2.25	2.35	2.31
2003	Mean (m s^{-1})	−0.92	−0.50	−0.57	−0.51	−0.55
	Rms (m s^{-1})	2.70	2.89	2.28	2.35	2.36
2004	Mean (m s^{-1})	−0.81	−0.37	−0.41	−0.35	−0.41
	Rms (m s^{-1})	2.49	2.21	2.23	2.31	2.23

5. Summary and discussion

This study analyzed four continually processed SST datasets (RYD, FNL, TIR, and MIR) for the period from 2002 to 2004 during July and August, the months when NAM develops to maturity. The results indicate that the values for different SST datasets vary somewhat, possibly because different algorithms and/or sensors were used. These variations from different datasets

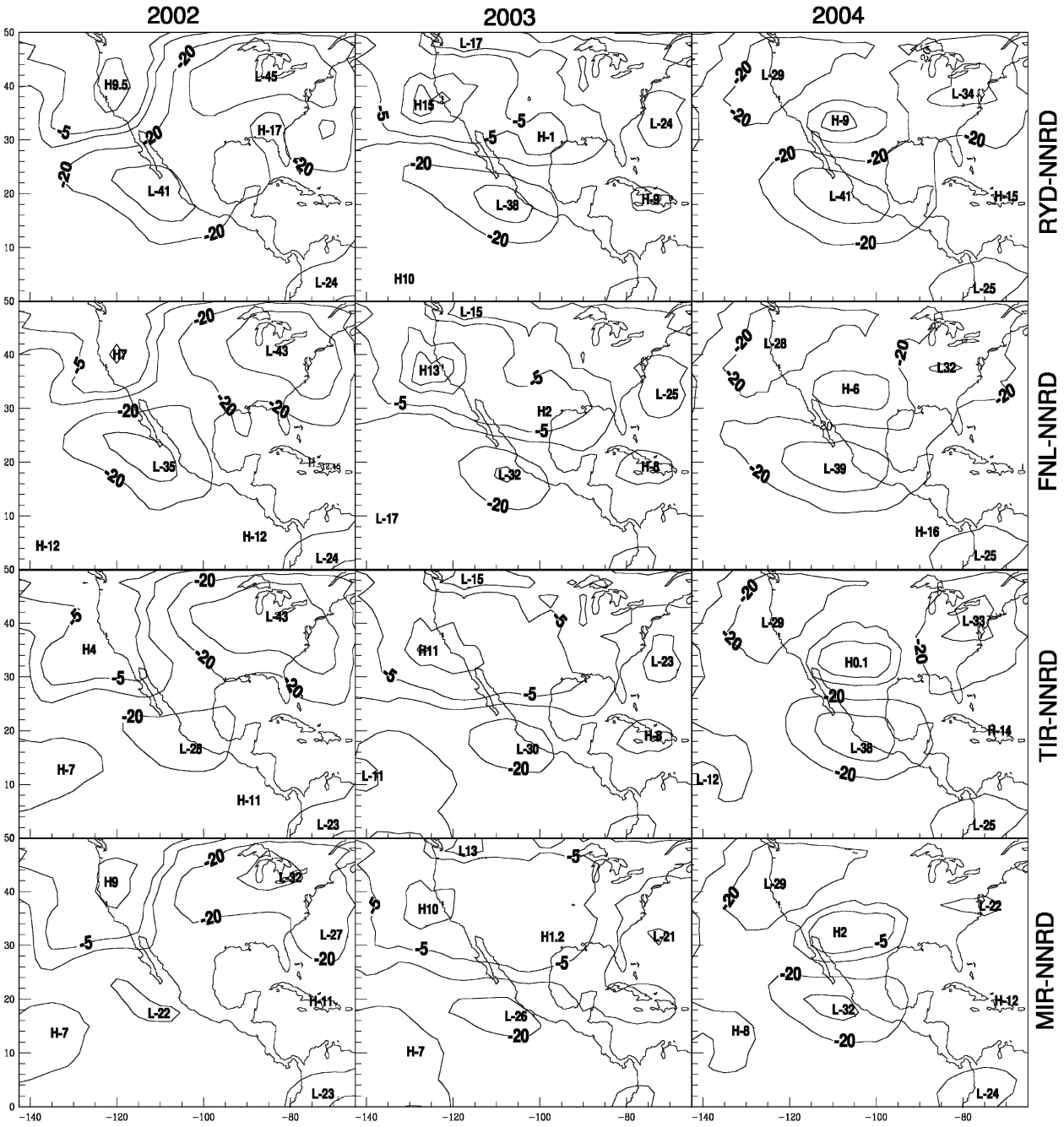

FIG. 9. Mean geopotential height differences between simulations and NNRD at 500 mb, respectively. The contours are −50, −30, −20, −10, −5, 5, 10, 20, 30, and 50 m.

are especially dominant in certain regions, such as the eastern Pacific and New England coastal regions.

Based on these SST differences, the study examined the sensitivities of MM5 simulations during the mature monsoon period in response to different SST source forcing. The studies indicate that under current modeling strategies, the following results are concluded from the 3-yr simulations:

1) The modeled rain-day ratios varied in phase and amplitude with model integration when different SST datasets were used, depending on which SST was used to drive the model. The model daily precipitation did not match the gauge/satellite observations day-to-day; however, in general, the model's variation trend was similar to that of the observations.

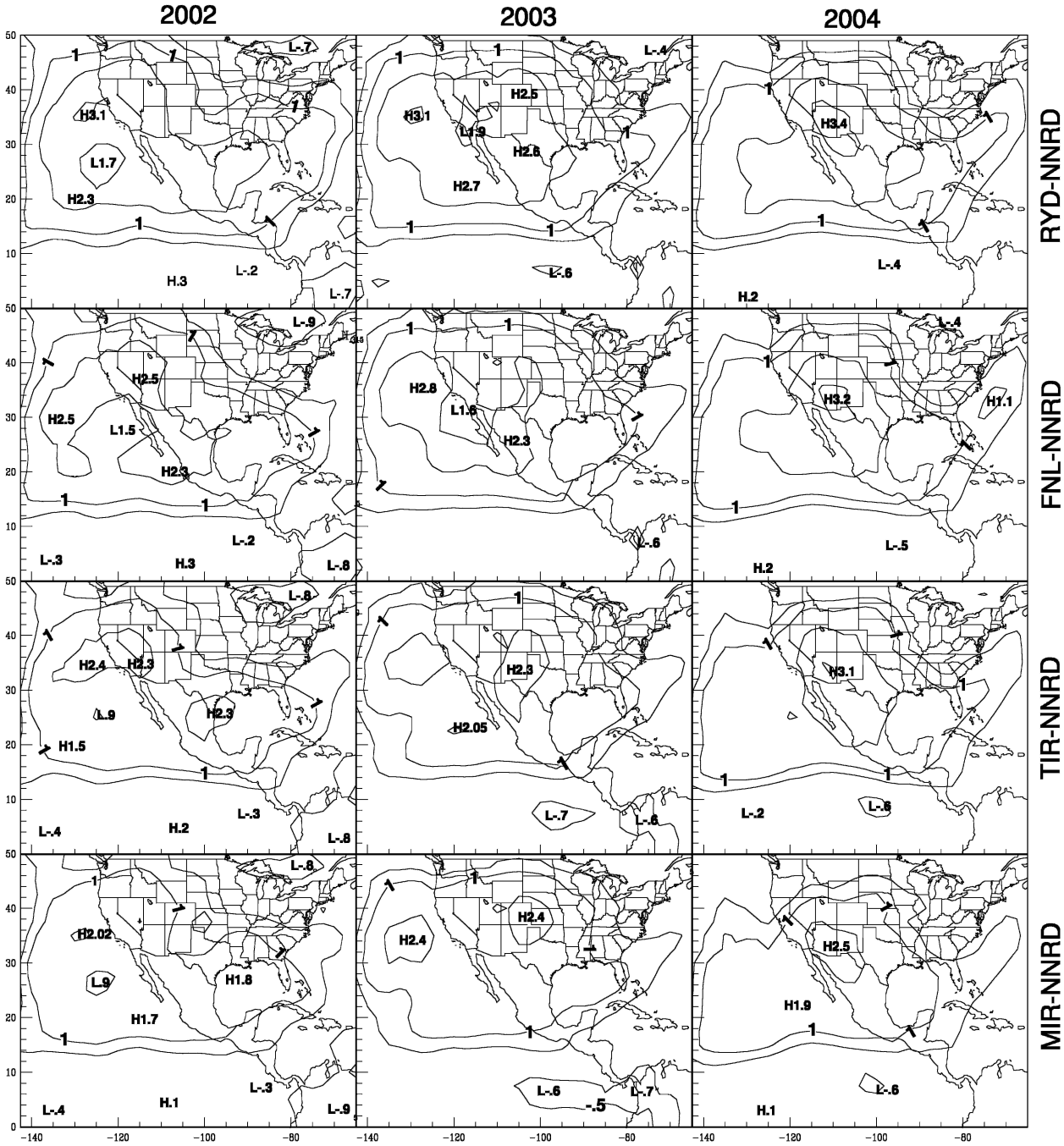

FIG. 10. Mean temperature differences between simulations and NNRD at 500 mb, respectively. The contours are −4°, −3°, −2°, −1°, −0.5°, 0.5°, 1°, 2°, 3°, and 4°C.

2) For the monthly mean, the model was able to generate similar mean precipitation and atmospheric circulation patterns when different SST datasets were used:
   (a) The model underestimated rainfall over the monsoon core, Oklahoma, Kansas, Lake Michigan, and its southern area, and the model overestimated rainfall over the offshore of southern Mexico, the Gulf of Mexico, the southern and eastern Mexican coasts, the Colorado Plateau, and the high-elevated Great Plains.
   (b) At 500 mb, the model generated similar atmospheric patterns but overestimated temperature at most domain areas and underrepresented the

geopotential height field in the whole domain, except in the northwestern United States in 2002 and 2003.

3) However, the model results do indicate some differences when different SST datasets were used to drive the model:
   (a) Comparing model simulations from different SST datasets with observational/analysis data at monthly scale showed that when MODIS *Aqua* midinfrared-retrieved SST was used to drive the model, the model statistically improved precipitation in the 3-yr simulations. Specifically, the rainfall estimate was a clear improvement over the offshore of southern Mexico, the Gulf of Mexico, and the southern and eastern Mexican coastal regions and was a small bias perturbation over the monsoon core, New Mexico, and the high-elevated Great Plains.
   (b) When MODIS *Aqua* SST datasets were used, modeling rainfall diurnal variation over the southwestern U.S. monsoon active region was more reasonable than those when RYD and FNL datasets were used.
   (c) When the midinfrared SST was used, the model estimates of geopotential height and temperature were closer to the analysis data in comparison with the results when the other SST dataset was used.

By using MIR SST forcing, model prediction errors were somewhat reduced. It is clear that certain errors stem from deficiencies in the model and cannot be removed by adjusting SST. Our previous study (Li at al. 2004) examined the reasons MM5 overestimated rainfall over the Gulf of Mexico and found that the model is unable to reproduce the low-level inversion above the marine boundary layers and therefore cannot generate enough convective inhibition to suppress the convection. Here, we checked model soundings in the eastern tropical Pacific at 10°N, 100°W at 1200 and 0000 UTC when RYD SST forced the model, which produced the highest rainfall, and when MIR SST forced the model, which produced the lowest rainfall. Both of these soundings showed high potential to develop convection rainfall: the CAPE forced by RYD SST was about 2500 J kg^{-1}, and the CAPE forced by MIR SST was about 1500 J kg^{-1}. The colder MIR SST at the location did decrease the CAPE value, but still could not reproduce the inversion above the marine boundary layer that had been observed in some experiments (e.g., Yin and Albrecht 2000). This model deficiency is partly due to weaknesses in the MRF PBL parameterization scheme that the experiments used. We have tested the effect of the PBL scheme on 2003 rainfall. By replacing the MRF PBL scheme with the Eta PBL parameterization scheme, the rainfall over the tropical region was further reduced although it was still overestimated in comparison with PERSIANN (not shown).

Acknowledgments. The comments and suggestions provided by two anonymous reviewers were extremely useful and helped the authors to improve and focus this paper. The first author also would like to thank Dr. Jimmy M. Ferng and other staff at the Computer Center and Information Technology, University of Arizona, for their help and support. Primary support for this research was provided under the NASA/EOS Interdisciplinary Research Program (NAG5-11044), the NOAA GAPP Program (NA16GP1605), and the NSF-STC Program (Agreement EAR-9876800).

REFERENCES

Adams, D. K., and A. C. Comrie, 1997: The North American monsoon. *Bull. Amer. Meteor. Soc.,* **78,** 2197–2213.

Anderson, B. T., and J. O. Roads, 2002: Regional simulation of summertime precipitation over the southwestern United States. *J. Climate,* **15,** 3321–3342.

Carleton, A. M., D. A. Carpenter, and P. J. Wesser, 1990: Mechanisms of interannual variability of the southwest United States summer rainfall maximum. *J. Climate,* **3,** 999–1015.

Castro, C. L., T. B. McKee, and R. A. Pielke Sr., 2001: The relationship of the North American monsoon to tropical and North Pacific sea surface temperatures as revealed by observational analyses. *J. Climate,* **14,** 4449–4473.

Cavazos, T., A. C. Comrie, and D. M. Liverman, 2002: Intraseasonal variability associated with wet monsoons in southwest Arizona. *J. Climate,* **15,** 2477–2490.

Chen, F., and J. Dudhia, 2001: Coupling an advanced land surface hydrology model with the Penn State–NCAR MM5 modeling system. Part I: Model implementation and sensitivity. *Mon. Wea. Rev.,* **129,** 569–585.

Dudhia, J., 1989: Numerical study of convection observed during the winter monsoon experiment using a mesoscale two-dimensional model. *J. Atmos. Sci.,* **46,** 3077–3107.

Farrara, J. D., and J. Yu, 2003: Interannual variations in the southwest U.S. monsoon and sea surface temperature anomalies: A general circulation model study. *J. Climate,* **16,** 1703–1720.

Gao, X., S. Sorooshian, J. Li, and J. Xu, 2003: SST data improve modeling of North American monsoon rainfall. *Eos, Trans. Amer. Geophys. Union,* **84,** P457, P462.

Garreaud, R. D., and J. M. Wallace, 1997: The diurnal march of convective cloudiness over the Americas. *Mon. Wea. Rev.,* **125,** 3157–3171.

Gochis, D. J., W. J. Shuttleworth, and Z.-Y. Yang, 2002: Sensitivity of the modeled North American monsoon regional climate to convective parameterization. *Mon. Wea. Rev.,* **130,** 1282–1298.

Guichard, F., D. B. Parsons, J. Dudhia, and J. Bresch, 2003: Evaluating mesoscale model predictions of clouds and radiation with SGP ARM data over a seasonal timescale. *Mon. Wea. Rev.,* **131,** 926–944.

Higgins, R. W., and W. Shi, 2000: Dominant factors responsible

for interannual variability of summer monsoon in the southwestern United States. *J. Climate,* **13,** 759–776.

——, and ——, 2001: Intercomparison of the principal modes of interannual and intraseasonal variability of the North American monsoon system. *J. Climate,* **14,** 403–417.

——, Y. Yao, and X. L. Wang, 1997: Influence of the North American monsoon system on the U.S. summer precipitation regime. *J. Climate,* **10,** 2600–2622.

——, Y. Chen, and A. V. Douglas, 1999: Interannual variability of the North American warm-season precipitation regime. *J. Climate,* **12,** 653–680.

Hong, S.-Y., and H.-L. Pan, 1996: Nonlocal boundary layer vertical diffusion in a medium-range forecast model. *Mon. Wea. Rev.,* **124,** 2322–2339.

——, and E. Kalnay, 2000: Role of sea surface temperature and soil moisture feedback in the 1998 Oklahoma–Texas drought. *Nature,* **408,** 842–844.

Kain, J. S., and J. M. Fritsch, 1990: A one-dimensional entraining/detraining plume model and its application in convective parameterization. *J. Atmos. Sci.,* **47,** 2784–2802.

Kalnay, E., and Coauthors, 1996: The NCEP/NCAR 40-Year Reanalysis Project. *Bull. Amer. Meteor. Soc.,* **77,** 437–471.

Kunkel, K. E., 2003: Sea surface temperature forcing the upward trend in U.S. extreme precipitation. *J. Geophys. Res.,* **108,** 4020, doi:10.1029/2002/JD002404.

Lau, K.-M., and C.-H. Sui, 1997: Mechanisms of short-term sea surface temperature regulation: Observations during TOGA COARE. *J. Climate,* **10,** 465–472.

Li, J., X. Gao, R. Maddox, and S. Sorooshian, 2004: Model study of evolution and diurnal variations of rainfall in the North American monsoon during June and July 2002. *Mon. Wea. Rev.,* **132,** 2895–2915.

Liang, X., L. Li, K. E. Kunkel, M. Ting, and J. X. L. Wang, 2004: Regional climate model simulation of U.S. precipitation during 1982–2002. Part I: Annual cycle. *J. Climate,* **17,** 3510–3529.

Mapes, B. E., T. T. Warner, M. Xu, and D. J. Gochis, 2004: Comparison of cumulus parameterization and entrainment using domain-mean wind divergence in a regional model. *J. Atmos. Sci.,* **61,** 1284–1295.

Markowski, G. R., and G. R. North, 2003: Climatic influence of sea surface temperature: Evidence of substantial precipitation correlation and predictability. *J. Hydrometeor.,* **4,** 856–877.

Mitchell, D. L., D. Ivanova, R. Rabin, T. J. Brown, and K. Redmond, 2002: Gulf of California sea surface temperatures and the North American monsoon: Mechanistic implications from observation. *J. Climate,* **15,** 2261–2281.

Mo, K. C., 2000: Intraseasonal modulation of summer precipitation over North America. *Mon. Wea. Rev.,* **128,** 1490–1505.

——, and J. N. Paegle, 2000: Influence of sea surface temperature anomalies on the precipitation regimes over the southwest United States. *J. Climate,* **13,** 3588–3598.

——, and H. M. Juang, 2003: Influence of sea surface temperature anomalies in the Gulf of California on North American monsoon rainfall. *J. Geophys. Res.,* **108,** 4112, doi:10.1029/2002JD002403.

——, J. N. Paegle, and R. W. Higgins, 1997: Atmospheric processes associated with summer floods and droughts in the central United States. *J. Climate,* **10,** 3028–3046.

Pastor, F., M. J. Estrela, D. Penarrocha, and M. M. Millan, 2001: Torrential rains on the Spanish Mediterranean coast: Modeling the effects of the sea surface temperature. *J. Appl. Meteor.,* **40,** 1180–1195.

Reynolds, R. W., N. A. Rayner, T. M. Smith, D. C. Stokes, and W. Wang, 2002: An improved in situ and satellite SST analysis for climate. *J. Climate,* **15,** 1609–1625.

Sorooshian, S., X. Gao, K. Hsu, R. A. Maddox, Y. Hong, H. V. Gupta, and B. Iman, 2002: Diurnal variability of tropical rainfall retrieved from combined GOES and TRMM satellite information. *J. Climate,* **15,** 983–1001.

Stensrud, D. J., R. L. Gall, S. L. Mullen, and K. W. Howard, 1995: Model climatology of the Mexican monsoon. *J. Climate,* **8,** 1775–1794.

Ting, M., and W. Wang, 1997: Summertime U.S. precipitation variability and its relation to Pacific sea surface temperature. *J. Climate,* **10,** 1853–1873.

Wang, W., and N. L. Seaman, 1997: A comparison study of the convective parameterization schemes in a mesoscale model. *Mon. Wea. Rev.,* **125,** 252–278.

Warner, T. T., B. E. Mapes, and M. Xu, 2003: Diurnal patterns of rainfall in northwestern South America. Part II: Model simulations. *Mon. Wea. Rev.,* **131,** 813–829.

Weller, R. A., and S. P. Anderson, 1996: Surface meteorology and air–sea fluxes in the western equatorial Pacific warm pool during the TOGA Coupled Ocean–Atmosphere Response Experiment. *J. Climate,* **9,** 1959–1990.

Woolnough, S. J., and J. M. Slingo, 2000: The relationship between convection and sea surface temperature on intraseasonal timescales. *J. Climate,* **13,** 2086–2104.

Yang, Z.-L., D. Gochis, W. Shuttleworth, and N.-Y. Niu, 2003: The impact of sea surface temperature on the North American monsoon: A GCM study. *Geophys. Res. Lett.,* **30,** 1033, doi:10.1029/2002GL015628.

Yin, B., and B. A. Albrecht, 2000: Spatial variability of atmospheric boundary layer structure over the eastern equatorial Pacific. *J. Climate,* **13,** 1574–1592.